



Heriot-Watt University

Heriot-Watt University
Research Gateway

Photoisomerization in a platinum-amido pincer complex

Zurek, Justyna M.; Paterson, Martin J

Published in:
Journal of Physical Chemistry Letters

DOI:
[10.1021/jz100156p](https://doi.org/10.1021/jz100156p)

Publication date:
2010

Document Version
Publisher's PDF, also known as Version of record

[Link to publication in Heriot-Watt Research Gateway](#)

Citation for published version (APA):
Zurek, J. M., & Paterson, M. J. (2010). Photoisomerization in a platinum-amido pincer complex: An excited-state reaction pathway controlled by localized ligand photochemistry. *Journal of Physical Chemistry Letters*, 1(9), 1301-1306. [10.1021/jz100156p](https://doi.org/10.1021/jz100156p)



General rights

Copyright and moral rights for the publications made accessible in the public portal are retained by the authors and/or other copyright owners and it is a condition of accessing publications that users recognise and abide by the legal requirements associated with these rights.

If you believe that this document breaches copyright please contact us providing details, and we will remove access to the work immediately and investigate your claim.

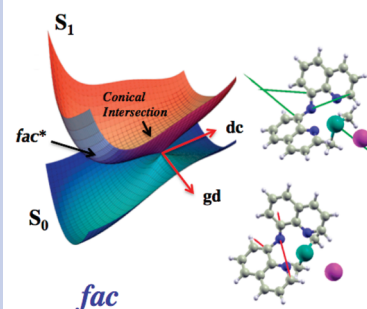
Photoisomerization in a Platinum—Amido Pincer Complex: An Excited-State Reaction Pathway Controlled by Localized Ligand Photochemistry

Justyna M. Żurek and Martin J. Paterson*

Department of Chemistry, School of Engineering and Physical Sciences, Heriot-Watt University, Edinburgh, Scotland EH14 4AS

ABSTRACT Computational investigations of the electronic spectroscopy and photochemical isomerization in the complex (bis(8-quinolynyl)amido)PtMe₂I are presented. Time-dependent density functional theory, in conjunction with the polarizable continuum solvent model, reproduce the experimental spectra for the mer and fac isomers well. The nature of the initially populated states for the mer isomer are $\pi\pi^*$ in nature and localized on the BQA ligand. Geometry optimization shows that the system relaxes in the excited manifold to a fac-like geometry in the S₁ electronic state. Complete active space self-consistent field (CASSCF) calculations show that there exists a sloped conical intersection that connects the excited- and ground-state fac species, allowing for radiationless deactivation in fac-like geometries.

SECTION Dynamics, Clusters, Excited States



The photochemistry of transition-metal complexes is an important subject that intersects many branches of science, including semiconductor technology,^{1–3} organic light-emitting diodes (OLED),^{4,5} C–H bond activation,^{6,7} biochemistry,^{8,9} and cell biology.¹⁰ From a fundamental point of view, there have been far fewer computational studies on light-induced inorganic chemistry than their organic counterparts. This is in part due to some of the extra complexities that arise in such systems, such as relativistic effects, degenerate and quasi-degenerate effects in a dense manifold of electronically excited states, and often the sheer system size, which precludes highly accurate computation. Nevertheless, in recent years, there have been significant studies that have highlighted the importance of a computational rationalization of experimental results in inorganic photochemistry.^{11–15}

In modeling organic photochemical reactions, ubiquitous features to emerge in recent years are conical intersection (seams).^{16–19} These regions of strong nonadiabatic coupling allow for ultrafast subpicosecond radiationless decay, and the topology around conical intersections affects the internal conversion dynamics of polyatomic molecules. Conical intersections also appear naturally in coordination complexes via the Jahn–Teller effect, where the two components of an electronically degenerate state give rise to the double cone potential energy surfaces in the space of the Jahn–Teller symmetry-breaking modes.^{14,20–22} Indeed, in recent years, it has become apparent that inorganic photochemistry involving the creation of coordinatively unsaturated species (e.g., metal carbonyl photodissociation²¹) provides a natural link between the photochemical and Jahn–Teller fields.^{20,22} General (nonsymmetry-imposed) intersections have been much less studied in inorganic chemistry.

We have computationally investigated a recent intriguing experimental result from Harkins and Peters.²³ They found that light irradiation of the complex (bis(8-quinolynyl)amido)PtMe₂I (bis(8-quinolynyl)amido = BQA) resulted in an unexpected stereochemical transformation from the meridional (mer) form (all coordinating nitrogens and metal being coplanar) to the facial (fac) form (all coordinating nitrogens cis to each other). The BQA ligand belongs to the group of robust “pincer-type” amido ligands that display a rich variety of chemistry.^{24–26} Transition-metal complexes with these ligands are very popular in organometallic and inorganic chemistry due to their potential applications in catalysis,^{27–29} electrochemical devices,³⁰ or the activation of small molecules.^{26,31} They can adopt a variety of geometries, from square-planar structures to more distorted ones.^{28,30,32–35} The common bonding feature of such complexes is that the metal is bonded to the quinolynyl arms via the nitrogen donor atoms and that the amide nitrogen is sp² hybridized, thus leading to significant conjugation through the π -system. Quinoline and related ligands showing ligand-localized photochemistry have been studied recently,^{5,36} with important consequences for use as OLEDs. We find that the photochemistry of the BQAPtMe₂I complex is dominated by localized chemistry on the BQA ligand, with the metal having very little effect on the nature of the electronic transitions. The initial excitation is of $\pi\pi^*$ type and involves a reduction in the conjugation across the planar amido linkage in the BQA. The system then relaxes in this state, with the ligand sphere

Received Date: February 4, 2010

Accepted Date: March 26, 2010

Published on Web Date: April 02, 2010

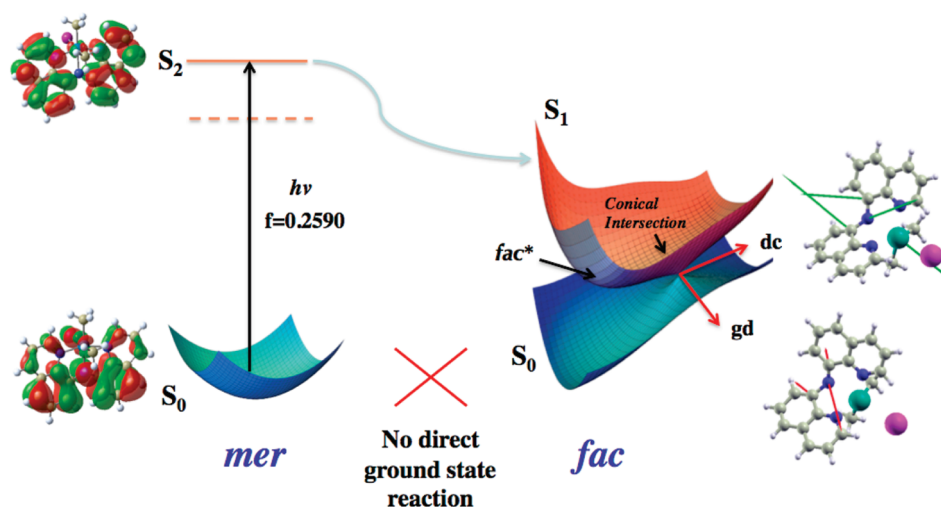


Figure 1. Schematic of *mer*–*fac* photoisomerization in (BQA)PtMe₂I involving localized $\pi\pi^*$ excitation on the BQA ligand, followed by relaxation to the S_1 *fac* minimum. Radiationless deactivation through a sloped conical intersection connecting the S_0 and S_1 states can then occur to lead to the stable *fac* photoproduct.

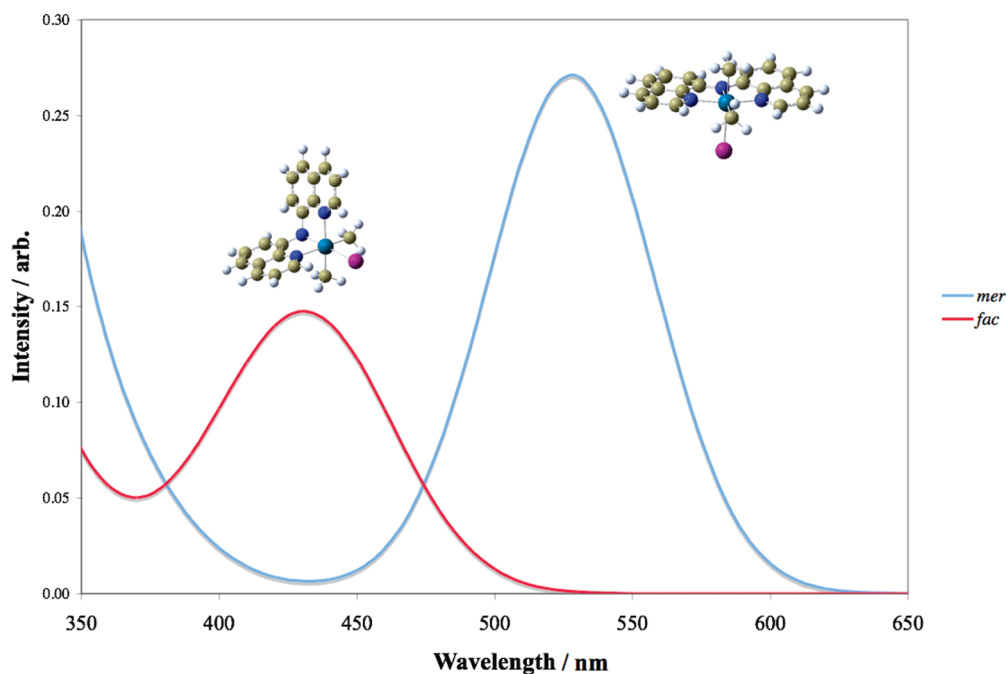


Figure 2. Simulated electronic spectra for the *mer* (blue) and *fac* (red) isomers of (BQA)PtMe₂I complex in CH₂Cl₂, obtained from PCM TD-B3LYP by applying a homogeneous Gaussian broadening to the lowest 60 electronically excited states.

undergoing rearrangement toward folded BQA conformations. This leads to an excited *fac* minimum, followed by a sloped conical intersection connecting the excited and ground electronic states (Figure 1), allowing for efficient radiationless deactivation to the ground-state *fac* geometry. This is a naturally occurring photochemical feature of the BQA ligand itself. This type of pathway may be potentially important for other complexes that involve the interesting family of flexible chelating pincer-type ligands.^{5,33,34,36,37}

The (BQA)PtMe₂I complex shows an unexpected coordination with a planar tridentate BQA in a *mer* geometry at the

octahedrally coordinated Pt(IV).²³ Harkins and Peters found this complex to be stable in acetone when stored in the dark but that it is unexpectedly transformed to the *fac* geometry under irradiation of light. The photoexcited *mer* form involves essentially a redistribution of the π system on the organic BQA ligand, which “loosens” the conjugation across the amide linkage (the amide nitrogen changes its hybridization from sp^2 to sp^3) and weakens the metal–BQA bonds via population of orbitals with nominal M– π antibonding character.

The simulated spectra are shown in Figure 2 (see Computational Details below). Here, the solvent in the PCM model is

Table 1. TD-B3LYP (PCM = CH₂Cl₂) Excitation Energies and Oscillator Strengths for Vertical Excitation of mer and fac Isomers^a

mer			fac		
state	<i>f</i>	character	state	<i>f</i>	character
S ₁ = 2.29 eV	0.0136	(H)(L) 0.121; (H)(L+1) 0.690	S ₁ = 2.78 eV	0.0033	(H)(L+1) 0.534; (H)(L+2) 0.443
S ₂ = 2.35 eV	0.2590	(H)(L) 0.693; (H)(L+1) −0.121	S ₂ = 2.85 eV	0.1178	(H)(L) 0.701
S ₃ = 2.79 eV	0.0023	(H)(L+2) 0.684	S ₃ = 3.03 eV	0.0366	(H)(L+1) −0.449; (H)(L+2) 0.537

^a Coefficients of principle particle–hole configurations in response eigenvectors relative to HOMO (H) and LUMO (L) are also given.

CH₂Cl₂, to match that used in ref 23. The effect of solvent is minimal, with only a small blue shift (on average, 0.05 eV) observed between the gas-phase and PCM results. We also note that the experimental photochemistry was performed in acetone, though the spectra were recorded in CH₂Cl₂, and we do not observe any difference in the computed spectra between these using the PCM model. The computed spectra compare favorably with the experimental ones. The mer form has an intense absorption at 534 nm, which is at 530 nm from TD-B3LYP. The fac form has a broad band centered at 422 nm, with a small shoulder at 510 nm. The TD-B3LYP gives this band maximum at 425 nm. The nature of the transitions that give rise to these bands can be determined by examination of the dominant particle–hole configurations of the response eigenvectors or similarly by determining the natural transition orbitals. We observed very little difference between analysis of the excitation using the canonical Kohn–Sham orbitals and the natural transition orbitals. The data given in Table 1 lists the dominant particle–hole configurations (using canonical orbitals) for the mer and fac isomers.

The important point with regards to the mer form is that the band at 530 nm (predominantly excitation to the S₂ state) involves essentially intraligand excitation of $\pi\pi^*$ type and not ligand-to-metal charge transfer (LMCT) as postulated previously.²³ The π^* orbital contains a very small component that is antibonding with respect to the t_{2g} metal d orbitals. The dominant feature of this state is charge redistribution on the BQA. The main particle–hole configuration of the state involves a donation of electron density from the central amide nitrogen to each π system on both adjacent quinoline rings. It is also worth noting that the lower dark state (S₁) and all higher dark states in the spectral range up to 400 nm involve this qualitative feature of localized ligand excitation, with charge redistribution across the BQA “backbone”.

The optimized geometries of the ground-state mer and fac structures are shown in Figure 3. These compare favorably with experimental structures. The mer isomer is 2.9 kcal mol^{−1} lower in energy than the fac using the PCM model, while for the gas-phase structures, the fac is 0.9 kcal mol^{−1} more stable. We were unable to find any evidence of a direct transition structure linking these two geometries on the S₀ potential surface. We suspect that any thermal process would have to go through (at least one) reactive intermediate via the dissociation of the iodine to give a five-coordinate species. The thermal isomerization is not seen experimentally.

In the S₂ state of the complex, relaxation involves the BQA ligand “folding” in, and the molecule relaxes to a quasi-fac form of the complex in the first singlet excited state (S₁) (Figure 3). The bright and dark states are very close and may

switch in energetic order with different DFT functionals (vide infra). If the ordering is correct and the bright state is S₂, then obviously, there must be a crossing between the S₁ and S₂ states. There is a minimum on the mer side of the reaction with BQA slightly nonplanar that is reached from the dark state. We were unable to locate an S₁ transition state due to the limitation of not having TD-DFT excited Hessians at present. Constrained geometry calculations indicate that any barrier will be relatively low. While the driving force in the populated S₂ state forces the system to relax toward fac-like geometries, obviously more accurate photochemical dynamics simulations would be required to determine if there is any population transfer to the dark state. However, whether via direct relaxation to the excited fac side of the reaction, or transformation over a barrier on a longer time scale, the system ends up at the same point, namely, the S₁ fac minimum (Figure 3). This fact is further emphasized if the bright and dark states are switched in order.

The TD-DFT and CASSCF excited geometry optimizations of this minimum are in good agreement. From this S₁ fac minimum, the excited molecule can access a conical intersection that connects the S₁ state to the ground state (shown schematically in Figure 1). This allows for radiationless relaxation to the ground-state fac geometry. The CASSCF energy difference between the S₁ minimum and the minimum-energy crossing point is around 10 kcal mol^{−1}, although, obviously, this value should be treated with caution due to incomplete accounting for dynamic correlation.

Interestingly, this conical intersection seam exists in the bare BQA ligand, and the excited relaxation and subsequent decay are essentially driven by the ligand’s photochemistry. CASSCF computations on the pure ligand indicate that at folded geometries, there is an extensive seam of intersection that connects the ground state with a $\pi\pi^*$ state. The global minimum-energy crossing point on this seam occurs at a CNC angle of 120°, but with the two quinoline groups twisted almost 90°. We have performed constrained conical intersection searches and observed that the intersection seam includes an energetically accessible portion with a small dihedral angle between quinoline groups. This constrained crossing point has a very similar geometry to the intersection in the full metal complex. From the geometries in Figure 3, it can be seen that the S₁ fac minimum occurs with a NpTN angle of 110°, which is more open than that at the conical intersection (92°) and that at the S₀ minimum (90°). Thus, molecular motion moves the system through the S₁ fac minimum, crosses from S₁ to S₀ via a radiationless transition in the conical intersection region, and finally relaxes to the stable S₀ fac minimum. The branching space for the conical intersection

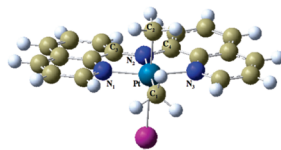
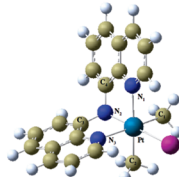
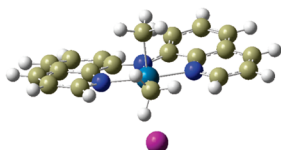
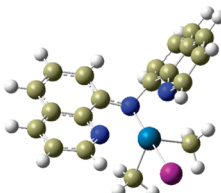
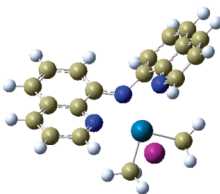
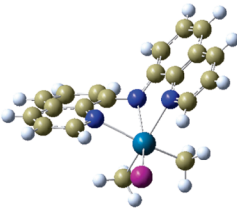
											
<i>mer</i>						<i>fac</i>					
<i>Gas phase (DFT)</i>						<i>Gas phase (DFT)</i>					
Pt-C ₁	Pt-C ₂	Pt-I	Pt-N ₁	Pt-N ₂	Pt-N ₃	Pt-C ₁	Pt-C ₂	Pt-I	Pt-N ₁	Pt-N ₂	Pt-N ₃
2.099	2.099	2.871	2.054	2.093	2.059	2.072	2.072	2.746	2.234	2.073	2.236
N ₁ -Pt-N ₃		C ₃ -N ₂ -C ₄		N ₂ -Pt-I		N ₁ -Pt-N ₃		C ₃ -N ₂ -C ₄		N ₂ -Pt-I	
161.80		133.14		91.33		97.21		118.15		174.89	
<i>Solvent- CH₂Cl₂ (DFT)</i>						<i>Solvent - CH₂Cl₂ (DFT)</i>					
Pt-C ₁	Pt-C ₂	Pt-I	Pt-N ₁	Pt-N ₂	Pt-N ₃	Pt-C ₁	Pt-C ₂	Pt-I	Pt-N ₁	Pt-N ₂	Pt-N ₃
2.100	2.086	2.953	2.062	2.089	2.058	2.072	2.073	2.777	2.226	2.064	2.229
N ₁ -Pt-N ₃		C ₃ -N ₂ -C ₄		N ₂ -Pt-I		N ₁ -Pt-N ₃		C ₃ -N ₂ -C ₄		N ₂ -Pt-I	
161.83		133.06		90.74		95.83		116.86		176.53	
											
<i>Mer - S₁ minimum TD-B3LYP</i>						<i>Fac - S₁ minimum TD-B3LYP</i>					
Pt-C ₁	Pt-C ₂	Pt-I	Pt-N ₁	Pt-N ₂	Pt-N ₃	Pt-C ₁	Pt-C ₂	Pt-I	Pt-N ₁	Pt-N ₂	Pt-N ₃
2.084	2.103	2.933	2.038	2.099	2.109	2.070	2.080	2.716	2.266	2.070	2.277
N ₁ -Pt-N ₃		C ₃ -N ₂ -C ₄		N ₂ -Pt-I		N ₁ -Pt-N ₃		C ₃ -N ₂ -C ₄		N ₂ -Pt-I	
132.54		160.94		91.65		99.55		119.15		169.52	
											
<i>Fac - S₁ minimum CASSCF(14,12)</i>						<i>Minimum Energy Conical Intersection CASSCF (14,12)</i>					
Pt-C ₁	Pt-C ₂	Pt-I	Pt-N ₁	Pt-N ₂	Pt-N ₃	Pt-C ₁	Pt-C ₂	Pt-I	Pt-N ₁	Pt-N ₂	Pt-N ₃
2.080	2.077	3.220	2.335	2.432	2.778	2.067	2.071	3.101	2.355	2.482	2.411
N ₁ -Pt-N ₃		C ₃ -N ₂ -C ₄		N ₂ -Pt-I		N ₁ -Pt-N ₃		C ₃ -N ₂ -C ₄		N ₂ -Pt-I	
99.66		127.52		150.37		92.61		125.72		153.24	

Figure 3. Optimized geometrical parameters for critical points involved in the mer–fac photoisomerization of (BQA)PtMe₂I. S₀ mer and S₀ fac optimized using B3LYP, both in the gas phase and with CH₂Cl₂ using the PCM model. S₁ fac optimized using TD-B3LYP and CASSCF; S₀/S₁ conical intersection optimized with CASSCF. Bond lengths are in Angstroms, angles in degrees.

is shown in Figure 1. This is the space (a 2D plane containing the derivative coupling (dc) and gradient difference (gd) vectors) in which the electronic degeneracy is lifted at first-order in vibrational motion. The motion is seen to mainly involve the amido link in the BQA ligand. Thus, one can see that when the locally excited ligand is driven toward such geometries, the crossing to the ground state becomes favorable.

The reaction path linking the conical intersection and the S₀ and S₁ fac minima (Figure 3) can be determined unambiguously by computing an intrinsic reaction coordinate (IRC). For this system, an IRC is computationally expensive,

but an idea of the downhill path from the conical intersection can be gained from examination of geometry optimization on the ground- and excited-state surfaces (using both CASSCF and (TD)-DFT). It is observed that the downhill direction from the conical intersection on S₁ leads directly to the S₁ fac minimum, while downhill on S₀ leads to the S₀ fac minimum. This is consistent with the observation that the conical intersection seam has a locally sloped topology, as depicted in Figure 1.

In summary, the metal complex acts as a scaffold for the pincer ligand, and localized excitation on the conjugated

ligand drives the intraligand folding, which takes the system downhill to the fac geometry. At such excited geometries, a conical intersection seam is accessible, which allows for radiationless decay to the stable fac photoproduct observed experimentally.

COMPUTATIONAL DETAILS

The ground-state isomeric forms were studied using density functional theory (DFT). For the DFT calculations, the one-electron basis set used was as follows: the Stuttgart Dresden effective core potential (SDD) on platinum (60 core electrons) and iodine (46 core electrons), in conjunction with the standard SDD valence basis and the 6-31G(d) basis on carbon, nitrogen, and hydrogen. The electronic spectroscopy was studied using time-dependent DFT. The effect of different functionals on excitation is given more fully in Supporting Information. The character of the lowest states contributing to the observed spectral bands involves $\pi\pi^*$ redistribution localized on the BQA ligand with all functionals investigated. Both B3LYP and PBE1PBE give the S_1 state as a dark state, with the bright S_2 very close (less than 0.07 eV). The functionals CAM-B3LYP and M06-2X give the opposite ordering of these states, although, again, they are very close and of the same character as that given by B3LYP and PBE1PBE. CAM-B3LYP and M06-2X show a blue shift of around 0.4 eV for the first peak in the spectrum. The lowest 60 electronic eigenstates were used to construct the spectrum by convoluting each transition with a Gaussian function (fwhm = 15 nm) to account for homogeneous line broadening (although we note that only a few states contribute in the low-energy region of interest). Geometry optimization in the excited manifold is now possible using analytical TD-DFT gradients,³⁸ which were used to study the relaxed excited-state geometries. Ground- and excited-state solvent effects were investigated using the B3LYP functional in conjunction with the polarizable continuum model (PCM),³⁹ with all the default settings as implemented in Gaussian 09. We note that optimized geometries in both the ground and excited states were found to be insensitive to the functional used. In order to investigate nonadiabatic relaxation pathways, we used complete active space self-consistent field (CASSCF) theory. Obviously, such a large system presents some difficulties in choosing an appropriate active space. Qualitatively, we looked at the TD-DFT orbitals involved in the photochemistry on both the reactant and product sides of the photoreaction. As discussed above, these were seen to involve ligand-centered π orbitals. Quantitatively, initial guess orbitals were natural orbitals from an unrestricted Hartree–Fock calculation. These are the orbitals which diagonalize the one-electron density matrix and whose eigenvalues are occupation numbers that give a measure of the importance of that orbital in a multiconfigurational wave function. From these, we generated active spaces consisting of 14 electrons distributed in 12 orbitals, generating 314028 singlet configurations. These CASSCF wave functions were checked for stability by switching some of the initial valence orbitals for alternative core or virtual orbitals and observing convergence to the same state. For the CASSCF calculations, the one-electron basis on platinum and iodine was as above,

while for carbon, nitrogen, and hydrogen the 3-21G(d) basis was used. For the conical intersection optimization with CASSCF, the orbital derivative terms were neglected in the solution of the coupled perturbed multiconfiguration self-consistent field (CP-MCSCF) equations. All DFT computations were performed with the Gaussian 09 program,⁴⁰ while the CASSCF calculations were performed with the Gaussian 03 program.⁴¹ All computations were performed on a Linux cluster with Intel Xeon Harpertown processors.

SUPPORTING INFORMATION AVAILABLE Cartesian coordinates, relative energies, and TD-DFT functional comparison. This material is available free of charge via the Internet at <http://pubs.acs.org>.

AUTHOR INFORMATION

Corresponding Author:

*To whom correspondence should be addressed. E-mail: m.j.paterson@hw.ac.uk.

ACKNOWLEDGMENT We thank the EPSRC for funding through Grant EP/F01709X.

REFERENCES

- (1) Burfeindt, B.; Hannappel, T.; Storck, W.; Willig, F. Measurement of Temperature-Independent Femtosecond Interfacial Electron Transfer from an Anchored Molecular Electron Donor to a Semiconductor as Acceptor. *J. Phys. Chem.* **1996**, *100*, 16463.
- (2) Hoffman, M. R.; Martin, S. T.; Choi, W.; Bahnemann, D. W. Environmental Applications of Semiconductor Photocatalysis. *Chem. Rev.* **1995**, *95*, 69–96.
- (3) Potje-Kamloth, K. Semiconductor Junction Gas Sensors. *Chem. Rev.* **2008**, *108*, 367–399.
- (4) Chi, Y.; Chou, P. T. Transition-Metal Phosphors with Cyclometalating Ligands: Fundamentals and Applications. *Chem. Soc. Rev.* **2010**, *39*, 638–655.
- (5) van Veldhoven, E.; Zhang, H.; Glasbeek, M. (Sub)picosecond Time-Resolved Fluorescence Depolarization of OLED Compounds Alq₃, Gaq₃, and Inq₃. In *Ultrafast Phenomena XII*; Elsaesser, T., Ed.; Springer: New York, 2001; pp 482–484.
- (6) Gunay, A.; Theopold, K. H. C–H Bond Activations by Metal Oxo Compounds. *Chem. Rev.* **2010**, *110*, 1060–1081.
- (7) Pitie, M.; Pratviel, G. Activation of DNA Carbon–Hydrogen Bonds by Metal Complexes. *Chem. Rev.* **2010**, *110*, 1018–1059.
- (8) McMillin, D. R.; McNett, K. M. Photoprocesses of Copper Complexes That Bind to DNA. *Chem. Rev.* **1998**, *98*, 1202–1219.
- (9) Szacilowski, K.; Macyk, W.; Drzewiecka-Matuszek, A.; Brindell, M.; Stochel, G. Bioinorganic Photochemistry: Frontiers and Mechanisms. *Chem. Rev.* **2005**, *105*, 2647–2694.
- (10) Haas, K. L.; Franz, K. J. Application of Metal Coordination Chemistry To Explore and Manipulate Cell Biology. *Chem. Rev.* **2009**, *109*, 4921–4960.
- (11) Daniel, C. Electronic Spectroscopy and Photoreactivity of Transition Metal Complexes. *Coord. Chem. Rev.* **2003**, *238*, 143–166.

- (12) Daniel, C. Electronic Spectroscopy and Photoreactivity of Transition Metal Complexes: Quantum Chemistry and Wave Packet Dynamics. *Top. Curr. Chem.* **2004**, *241*, 119–165.
- (13) Paterson, M. J.; Blancafort, L.; Wilsey, S.; Robb, M. A. Photo-induced Electron Transfer in Squaraine Dyes: Sensitization of Large Band Gap Semiconductors. *J. Phys. Chem. A* **2002**, *106*, 11431–11439.
- (14) Paterson, M. J.; Hunt, P. A.; Robb, M. A.; Takahashi, O. Non-Adiabatic Direct Dynamics Study of Chromium Hexacarbonyl Photodissociation. *J. Phys. Chem. A* **2002**, *106*, 10494–10504.
- (15) Worth, G. A.; Welch, G.; Paterson, M. J. Wavepacket Dynamics Study of $\text{Cr}(\text{CO})_5$ after Formation by Photodissociation: Relaxation through an $(E \oplus A) \otimes e$ Jahn–Teller Conical Intersection. *Mol. Phys.* **2006**, *104* (5–7), 1095–1105.
- (16) Garavelli, M. Computational Organic Photochemistry: Strategy, Achievements and Perspectives. *Theor. Chem. Acc.* **2006**, *116*, 87–105.
- (17) Robb, M. A.; Bernardi, F.; Olivucci, M. Conical Intersections as a Mechanistic Feature of Organic-Photochemistry. *Pure Appl. Chem.* **1995**, *67*, 783–789.
- (18) Robb, M. A.; Garavelli, M.; Olivucci, M.; Bernardi, F. A Computational Strategy for Organic Photochemistry. *Rev. Comput. Chem.* **2000**, *15*, 87–146.
- (19) Yarkony, D. R. Conical Intersections: The New Conventional Wisdom. *J. Phys. Chem. A* **2001**, *105*, 6277–6293.
- (20) Paterson, M. J.; Bearpark, M. J.; Robb, M. A.; Blancafort, L.; Worth, G. A. Conical Intersections: A Perspective on the Computation of Spectroscopic Jahn–Teller Parameters and the Degenerate 'Intersection Space'. *Phys. Chem. Chem. Phys.* **2005**, *7*, 2100–2115.
- (21) Mckinlay, R. G.; Paterson, M. J. The Jahn–Teller Effect in Binary Transition Metal Carbonyl Complexes. In *The Jahn–Teller Effect: Fundamentals and Implications for Physics and Chemistry*; Köppel, H., Yarkony, D. R., Barentzen, H., Eds.; Springer-Verlag: Heidelberg, Germany, 2010; pp 311–344.
- (22) Bersuker, I. B. *The Jahn–Teller Effect*; Cambridge: New York, 2006.
- (23) Harkins, S. B.; Peters, J. C. Unexpected Photoisomerization of a Pincer-Type Amido Ligand Leads to Facial Coordination at $\text{Pt}(\text{IV})$. *Inorg. Chem.* **2006**, *45*, 4316–4318.
- (24) Fryzuk, M. D. Excursions around the Periodic Table: Ligand Design in Inorganic Chemistry. *Can. J. Chem.* **1992**, *70*, 2839–2845.
- (25) Peters, J. C.; Harkins, S. B.; Brown, S. D.; Day, M. W. Pincer-Like Amido Complexes of Platinum, Palladium, And Nickel. *Inorg. Chem.* **2001**, *40*, 5083–5091.
- (26) Van Koten, G. Tuning the Reactivity of Metals Held in a Rigid Ligand Environment. *Pure Appl. Chem.* **1989**, *61*, 1681–1694.
- (27) Huang, M. H.; Liang, L. C. Amido Pincer Complexes of Palladium: Synthesis, Structure, And Catalytic Heck Reaction. *Organometallics* **2004**, *23*, 2813–2816.
- (28) Sun, K.; Wang, L.; Wang, Z. Synthesis and Characterization of Amido Pincer Complexes of Lithium and Nickel and Catalysis of the Nickel Complexes in the Kumada Cross-Coupling. *Organometallics* **2008**, *27*, 5649–5656.
- (29) Weng, W.; Guo, C. Y.; Celenligil-Cetin, R.; Foxman, B. M.; Ozerov, O. V. Skeletal Change in the PNP Pincer Ligand Leads to a Highly Regioselective Alkyne Dimerization Catalyst. *Chem. Comm.* **2006**, 197–199.
- (30) Harkins, S. B.; Peters, J. C. A Highly Emissive Cu_2N_2 Diamond Core Complex Supported by a $[\text{PNP}]^-$ Ligand. *J. Am. Chem. Soc.* **2005**, *127*, 2030–2031.
- (31) Harkins, S. B.; Peters, J. C. Base-Promoted Benzene C–H Activation Chemistry at an Amido Pincer Complex of Platinum(II). *Organometallics* **2002**, *21*, 1753–1755.
- (32) Betley, T. A.; Qian, B. A.; Peters, J. C. Group VIII Coordination Chemistry of a Pincer-Type Bis(8-quinolinyl)amido Ligand. *Inorg. Chem.* **2008**, *47*, 11570–11582.
- (33) Fout, A. R.; Basuli, F.; Fan, H.; Tomaszewski, J.; Huffman, J. C.; Baik, M.; Mindiola, D. J. A Co_2N_2 Diamond-Core Resting State of Cobalt^(I): A Three-Coordinate CoI Synthon Invoking an Unusual Pincer-Type Rearrangement. *Ang. Chem., Int. Ed.* **2006**, *45*, 3291–3295.
- (34) Harkins, S. B.; Peters, J. C. Amido-Bridged Cu_2N_2 Diamond Cores That Minimize Structural Reorganization and Facilitate Reversible Redox Behavior between a $\text{Cu}^{\text{I}}\text{Cu}^{\text{I}}$ and a Class III Delocalized $\text{Cu}^{(1.5)}\text{Cu}^{(1.5)}$ Species. *J. Am. Chem. Soc.* **2004**, *126*, 2885–2893.
- (35) Maiti, D.; Paul, H.; Chanda, N.; Chakraborty, S.; Mondal, B.; Puranik, V. G.; Lahiri, G. K. Synthesis, Structure, Spectral and Electron-Transfer Properties of Octahedral- $[\text{Co}^{\text{III}}(\text{L})_2]^+ / [\text{Zn}^{\text{II}}(\text{L})_2]$ and Square Planar- $[\text{Cu}^{\text{II}}(\text{L})\{\text{OC}(\text{=O})\text{CH}_3\}]$ Complexes Incorporating Anionic Form of Tridentate Bis(8-quinolinyl)amine $[(\text{N}^1\text{C}_9\text{H}_6)\text{-N}^2\text{-C}_9\text{H}_6\text{N}^3, \text{L}^-]$ Ligand. *Polyhedron* **2004**, *23*, 831–840.
- (36) Humbs, W.; van Veldhoven, E.; Zhang, H.; Glasbeek, M. Sub-Picosecond Fluorescence Dynamics of Organic Light-Emitting Diode Tris(8-hydroxyquinoline) Metal Complexes. *Chem. Phys. Lett.* **1999**, *304*, 10–18.
- (37) Doux, M.; Mézailles, N.; Ricard, L.; Le Floch, P.; Vaz, P. D.; Calhorda, M. J.; Mahabiersing, T.; Hartl, F. Syntheses, X-ray Structures, Photochemistry, Redox Properties, and DFT Calculations of Interconvertible fac- and mer- $[\text{Mn}(\text{SPS})(\text{CO})_3]$ Isomers Containing a Flexible SPS-Based Pincer Ligand. *Inorg. Chem.* **2005**, *44*, 9213–9224.
- (38) Scalmani, G.; Frish, M. J.; Mennucci, B.; Tomasi, J.; Cammi, R.; Barone, V. Geometries and Properties of Excited States in the Gas Phase and in Solution: Theory and Application of a Time-Dependent Density Functional Theory Polarizable Continuum Model. *J. Chem. Phys.* **2006**, *124*, 94107.
- (39) Scalmani, G.; Frisch, M. J. Continuous Surface Charge Polarizable Models of Solvation I. General Formalism. *J. Chem. Phys.* **2010**, *132*, 114110.
- (40) Frisch, M. J.; Trucks, G. W.; Schlegel, H. B.; Scuseria, G. E.; Robb, M. A.; Cheeseman, J. R.; Scalmani, G.; Barone, V.; Mennucci, B.; Petersson, G. A.; et al. *Gaussian 09*, Revision A.02; Gaussian, Inc.: Wallingford, CT, 2009.
- (41) Frisch, M. J.; Trucks, G. W.; Schlegel, H. B.; Scuseria, G. E.; Robb, M. A.; Cheeseman, J. R.; Montgomery, J. A., Jr.; Vreven, T.; Kudin, K. N.; Burant, J. C.; et al. *Gaussian 03*, revision D.01; Gaussian, Inc.: Wallingford, CT, 2004.